NETWORK-BASED EQUITY EVALUATION OF TSUNAMI EVACUATION ACCESS FOR A MEGATHRUST SCENARIO IN PALABUHANRATU

Reno Sudibyo[1,2]*, Anwar Kurniadi[1], Adi Subiyanto[1], Fajar Gilang Ramadhan[1,2]
[1]Disaster Management Study Program, Faculty of National Security, The Republic of Indonesia Defense University, Kawasan IPSC Sentul, Indonesia
[2]Indonesian Agency for Meteorological, Climatological and Geophysics, Indonesia
***E-mail:** *reno.sudibyo@bmkg.go.id*

Received: October 7, 2025 Reviewed: October 10, 2025 Accepted: November 12, 2025

ABSTRACT

We present a network-based equity evaluation of tsunami evacuation access for a Palabuhanratu megathrust scenario, quantifying who can reach safety in time and how this access is distributed. Physics-based inundation is overlaid with a road graph to compute multimodal time-to-safety and isochrones (maps of equal travel time). Village-level access is summarized with overall reachability (RR), Gini, and a hazard-weighted Gini (Gini*). Evacuation time allowances (ETAs) are set to 22, 18, and 15 minutes, validated against site-specific arrival time modeling [36], and observed 2-6 minute real-world departures in the 2024 Noto event [3]. Results reveal a temporal tipping: at ETA = 22 min, all at-risk origins reach a tsunami evacuation area (TEA) (RR=1.00) with low inequality; tightening to 18 and 15 min sharply reduces RR and increases Gini*. Adding one alternative TEA (Smile Hill, a candidate site on a local ridge) yields localized time savings and small positive ΔRR in specific clusters at 22 minutes but no systemwide change at 18 or 15 minutes, indicating time scarcity dominates access in tight windows. Methodologically, our design follows beat-the-wave logic (ensuring travel time is less than wave arrival time) and least-/shortest-cost routing on OSMnx/NetworkX graphs [28–29], producing a reproducible screening tool that joins access, fairness, and hazard emphasis for TEA design under time-critical evacuation.

Keywords: tsunami evacuation; network-based equity; overall reachability (RR); Gini; Gini*; isochrones; Palabuhanratu; beat-the-wave.

1. Introduction

Near-field tsunamis leave only minutes for protective action; in such settings, time-to-safety and the structure of local road networks largely determine who can reach tsunami evacuation areas (TEAs) before wave arrival [1]–[3]. Conventional hazard maps emphasize inundation depth and extent, yet they do not directly communicate whether at-risk residents can evacuate in time or how access is distributed across settlements. In particular, prior studies seldom report coverage and equity in one comparative frame or apply hazard-weighted fairness, leaving the spatial fairness question underdeveloped for near-field design. A network-based evacuation perspective closes this gap by coupling physics-based inundation with multimodal travel times and isochrones to summarize accessibility at administratively meaningful units (e.g., villages) [1]–[3]. Palabuhanratu—an urbanizing coastal district on the south coast of West Java—offers a relevant near-field context to test such an approach, where local relief, arterial geometry, and settlement patterns interact with short warning windows and arrival guidance on the order of ~20–25 minutes that motivates the 22→18→15-minute windows used here [36]; for planning guidance see [22].

Building on recent beat-the-wave (BTW) mapping and path-distance/ETE evidence that modest lead-time changes can decisively alter outcomes [7]–[10], [13], [14], [36] we frame evacuation as a time-budget problem over the road network for walking and driving. Travel times and flow-path–consistent reachability are computed from origin nodes to the nearest TEA and read against an ETA (evacuation time allowance). To diagnose distributional fairness, we pair an overall reachability ratio (RR: the fraction of at-risk origins whose travel time does not exceed the budget) with the Gini coefficient of access and a hazard-weighted variant (Gini*), Implementation uses an OSM-derived network with OSMnx/NetworkX [28–29] and, for comparability and reproducibility, we adopt a constant baseline walking speed and uncongested driving; robustness is documented in the Supplement via a grade-modulated walking sensitivity and targeted capacity/queue penalties at critical bridges/intersections, which keep shortfalls in higher-exposure villages visible in summary statistics [2], [3]. The tsunami source is an interface-thrust elastic dislocation (depth 20 km, strike 324°, dip 8°, rake 96°), on a 119 km × 53.5 km rectangular plane with 2.2 m uniform slip (Mw≈7.7), placed at 3.487° S, 100.082° E. The simulation was run for 7200 s using a nested grid structure, starting from a 1 arc-minute parent grid and progressing through six layers to a final runup grid resolution of 1/405 arc-minute (approx. 4.6 m). Within this frame we contrast the existing TEA configuration (baseline) with a plausible alternative (Smile Hill), a candidate TEA on a local ridge used here as a realistic siting test, which was selected as the top-performing candidate from a quantitative "what-if" analysis (see Supplementary Material 1). This analysis ranked potential sites based on maximizing overall reachability ΔRR for walking at ETA = 22. Then we examine three Evacuation time allowances representative of near-field windows—22, 18, and 15 minutes—which bracket an upper-bound “access plateau” and progressively tighter constraints consistent with BTW/path-distance practice [7]–[10], [13], [14], [21], [5].

Thus, the manuscript advances a compact and interpretable screening lens for near-field evacuation in Palabuhanratu: it integrates physics-based inundation with network travel times, summarizes access and equity at the village scale through the RR–Gini–Gini* triad, and compares a baseline TEA layout with a realistic alternative under time budgets that reflect contemporary guidance and empirics. By reading coverage and equity jointly—and by situating results within the 18–22-minute timing logic documented in recent studies—this introduction sets up the central question that runs through the paper: when does a new site meaningfully expand who reaches safety, and where do gains or shortfalls concentrate across villages, given the severe time constraints of near-field tsunamis [1]–[6], [7]–[10], [13], [14]?.

2. Data and Methods

This study builds a reproducible, network-based pipeline that fuses a physics-based tsunami inundation field with a multimodal road graph to estimate time-to-safety and evaluate equity of access at the village scale. The analysis compares the baseline set of tsunami evacuation areas (TEAs) with a plausible alternative (Smile Hill) under three evacuation-time allowances (ETAs) of 22, 18, and 15 minutes, chosen to bracket a locally feasible plateau near first arrivals and progressively tighter near-field decision windows [1]–[3], [7]–[9], [13], [14]. The case setting is Palabuhanratu (West Java, Indonesia), a near-field coastline fronting the Indian Ocean; all layers are harmonized to EPSG:32748 (UTM 48S) and computations use meters/minutes. Outputs are comparative indicators (not absolute forecasts), consistent with rapid-screening practice in tsunami-evacuation studies [2], [7], [36].

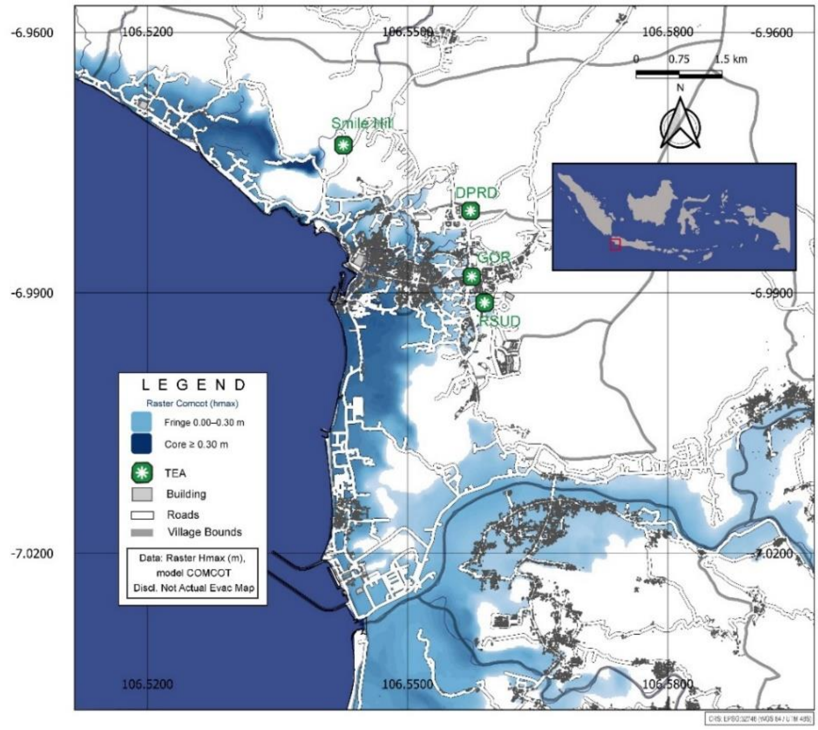

Figure 1. Maximum water height (h_{max}, meters) for the Palabuhanratu tsunami scenario prepared in QGIS (CRS EPSG:32748, UTM 48S). The raster shows h_{max} shading with two operational cutoffs—≥0.00 m and ≥0.30 m—used to define the at-risk domain for tagging road-graph origins. These thresholds are carried through to the network-based equity analysis (RR, Gini, and hazard-weighted Gini*), where h_{max} functions as a reproducible hazard input while the main text focuses on comparative access and equity indicators.

The inundation forcing is a COMCOT maximum water-height hmax for a Palabuhanratu megathrust scenario; COMCOT solves the nonlinear shallow-water equations with optional nesting for generation–propagation–run-up [1], [2]. The tsunami source is an interface-thrust elastic dislocation (depth 20 km, strike 324°, dip 8°, rake 96°), on a 119 km × 53.5 km rectangular plane with 2.2 m uniform slip; the rupture is placed at 3.487° S, 100.082° E and imposed at t = 0 s. Assuming $\mu \approx 3\times10^{10}$ Pa gives $M_0 \approx 4.2\times10^{20}$ N·m (Mw≈7.7). Landslide forcing and external wave-maker initializations are not used; the initial free-surface is from the fault uplift. For robustness we analyze two cut-offs on hmax : ≥0.00 m and ≥0.30 m. Each raster is thresholded, vectorized (polygonized), dissolved to a multipart geometry, and reprojected to EPSG:32748; sub-cell slivers are removed. A directed road graph G=(N,E) is then constructed from OpenStreetMap (OSM) with ODbL attribution [27]. OSMnx downloads footprints [28] and simplifies topology (e.g., consolidates degree-2 chains and removes self-loops/duplicates); NetworkX provides shortest-path primitives on the same vertex set [29]. All graph nodes inside the active inundation polygon are tagged as at-risk origins (preserving local street geometry). TEAs are modeled as points without capacity/queuing; we analyze (i) Baseline TEAs and (ii) Baseline + Smile Hill (one added TEA), with each destination snapped to its nearest reachable graph node [29].

The ETA windows reflect contemporary guidance and empirics. Around 22 minutes, first significant arrivals at many Cascadia- and Indonesia-style sites occur on the order of ∼20−25 minutes, placing ≈ 22 minutes near the upper bound of feasible self-evacuation before wave arrival [2], [7], [11]–[14], then We evaluate three ETAs (time budgets): 22, 18, and 15 minutes. While our COMCOT simulation was configured to provide the Hmax inundation mask, the 22-minute upper bound is validated by independent, site-specific modeling. A recent COMCOT study modeling a megathrust scenario for Palabuhanratu explicitly calculates the first tsunami arrival time at 22 minutes [36] BTW (beat-the-wave) mapping formalizes this through minimum-speed-to-safety or least-cost-time fields against wave-arrival isolines; near 22 minutes many origins cross from non-reachable to reachable, producing an access plateau [21], [5]. National path-distance assessments and regional ETE studies show that modest reductions from ∼22 to ≈ 18 trigger sharp drops in the share of residents reaching high ground, especially where slopes, circuitous streets, or bridge chokepoints add friction [7], [10]. Under ≈15 minutes, near-field constraints dominate; even small departure delays—e.g., ∼2−6 minutes documented for the 2024 Noto Peninsula tsunami from large-scale smartphone geolocation—leave little residual travel time, producing pronounced reductions in reachability despite local routing improvements or a single additional TEA [3], [7], [10], [14]. In practice, tight windows are often operationalized using 10/15/20-minute departure constructs to stress-test plans [13]. These windows are commonly used for operational stress testing [22] (see also examples in [21]), Formally, with origin-specific travel time t_i, the reachable fraction at budget T is

$$\boldsymbol{R(T)} = \frac{\mathbf{1}}{|\boldsymbol{A}|}\sum_{\boldsymbol{i}\in \boldsymbol{A}} \mathbf{1}\{\boldsymbol{t_i} \le \boldsymbol{T}\} \qquad (1)$$

which is sigmoid-like around 15–22 minutes in near-field contexts; the marginal gain ∂R/∂T is largest between ∼18−22 minutes and near zero once a plateau at R≈1 (or a decline toward R≈0) is approached [7]–[10], [13], [14]. These properties motivate the triad ETA = 22 min, 18, 15 minutes [36].

Travel times are computed on *G* using mode-specific link speeds. For each edge $e \in E$ with length $L_{e(m)}$ and mode speed v_e(m/min), the edge time is

$$\boldsymbol{\tau_e} = \frac{\boldsymbol{L_e}}{\boldsymbol{v_e}} \qquad (2)$$

Walking adopts a nominal baseline $v_{walk} = 3.0\ km\ h^{-1}$ (50 m/min); a $2.0–3.5\ km\ h^{-1}$ sweep probes robustness and aligns with recent evacuation modelling [2], [7]–[10]. Driving uses OSM maxspeed where present; otherwise defaults by road class approximate free-flow (no congestion/blockages). For origin *i*, the time to the nearest TEA is

$$\boldsymbol{t_i} = \boldsymbol{min}_{\boldsymbol{p}\in \boldsymbol{P(i,D)}} \sum_{\boldsymbol{e}\in \boldsymbol{p}} \boldsymbol{\tau_e} \qquad (3)$$

Because pedestrian velocity in reality is heterogeneous**,** we interpret v_{walk} as a screening anchor**.** Speeds vary with demography (older adults, children, persons with disabilities, group movement, carried loads) and with terrain (grade, surface condition). Empirical and agent-based studies report slower and more variable paces for vulnerable groups and mixed-ability cohorts, with pre-movement and coordination adding nontrivial dispersion to departure and travel times [4], [7], [18]. Topographic slope further modulates feasible speeds; path-distance formulations routinely reduce effective velocity as grade increases, which contracts isochrones relative to flat-ground approximations [5]. A compact expression is $v_{walk\ (X)} = v0\phi(\nabla z(x))$, where $\phi(\cdot)$ is monotone-decreasing in local grade and v_0 reflects cohort-specific baselines. While the present model uses a constant v_0 for clarity and comparability across scenarios, these heterogeneities imply that village-level access and equity are sensitive to demographic mix and slope patterns; introducing $v_{walk\ (X)}$ would likely shrink reachable envelopes in steep sectors and widen the dispersion of travel times around the plateau window [4], [5], [7], [18].

Equity is summarized at the village level. Let $nv = |Av|$ be the number of at-risk origins in village v (with

$A_v = A \setminus \cap\ v), r_v = |\{i \in A_v : t_i \leq ETA\}|$, and $RR_v = \frac{r_v}{n_v}$ (for $n_v > 0$) The overall reachability

$$\boldsymbol{RR_{overall}} = \frac{\sum_v \boldsymbol{r_v}}{\sum_v \boldsymbol{n_v}} \tag{4}$$

and inequality of access is measured with a Gini coefficient that weights villages by at-risk counts. Sorting villages by non-decreasing RR_v with weights $w_v = n_v$, define

$$\boldsymbol{W_k} = \frac{\sum_{j=1}^{k} \boldsymbol{w(j)}}{\sum_{j=1}^{m} \boldsymbol{w(j)}}, \boldsymbol{V_k} = \frac{\sum_{j=1}^{k} \boldsymbol{w(j)w(j)RR(j)}}{\sum_{j=1}^{m} \boldsymbol{w(j)w(j)RR(j)}} \tag{5}$$

The Lorenz curve is the polyline through (W_k, V_k); the Gini is

$$\boldsymbol{Gini} = \boldsymbol{1} - \boldsymbol{2}\sum_{k=1}^{m} \frac{\boldsymbol{1}}{\boldsymbol{2}} (\boldsymbol{V_k} + \boldsymbol{V_{k-1}})(\boldsymbol{W_k} - \boldsymbol{W_{k-1}}) \tag{6}$$

Standard in transportation-equity diagnostics [15], [16]. To emphasize fairness where exposure is higher, we compute a Gini* by replacing w_v with $w_v = n_v \bar{h}_v$, where $\bar{h}_v$ to is the mean h_{max} in village v above the active cutoff, normalized to [0,1] [12], [13]. Because inequality in effort (travel time) may persist when $RR_{overall} = 1.00$, we also tabulate CDFs and Lorenz curves of $\{t_i\}$ over A [2], [7].

The scenario matrix is a full factorial by mode (walk/drive), ETA (22/18/15), inundation cutoff (0.00/0.30 m), and TEA configuration (Baseline vs. Baseline+Smile Hill). For each cell we produce: (i) $RR_{overall}$, Gini**,** Gini*; (ii) village tables (RR_v) and ΔRR_v (Smile Hill − Baseline); and (iii) figures (CDFs, isochrones, and RR_v and ΔRR_v maps). We also sweep walking speeds 2.0–3.5 km h^{-1} to probe robustness in line with least/shortest-cost and ETE practices [7]–[10], [15], [16]. The software stack ensures reproducibility: vector/raster ops use GeoPandas, Shapely**,** PyOgrio/Fiona**,** Rasterio; CRS handling uses pyproj/PROJ; graphs & routing rely on OSMnx (download/topology) and NetworkX (Dijkstra); numerics/plots use NumPy**,** Pandas, and Matplotlib. Implementation is in Python 3.11 with pinned versions; scripts expose CLI flags for ETA, cutoff, CRS, and I/O paths [5], [6], [17]–[22]. Quality assurance includes CRS harmonization, topology checks (no orphan components; degree-2 simplification within tolerance), raster-to-vector consistency, and overlays that verify inundation-edge alignment with the road network.

Finally, we make explicit the assumptions and method-linked limitations. The analysis is a deterministic free-flow screening: a single h_{max} surface per cutoff (no ensemble), static networks without incident blockages, and no capacity or congestion dynamics on links or at intersections. A single global ETA is used in lieu of spatially varying arrival-time fields. These simplifications isolate the role of time-to-safety and lead-time compression and are consistent with rapid appraisal and national path-distance analyses foregrounding departure delays [7], [9], [10]. However, they create a downward bias in (4) inequality for the driving mode: in real evacuations, finite saturation flows, signal timing, turn-pocket spillback, lane losses, bridge bottlenecks, and queuing at merge points increase travel times heterogeneously across villages; agent-based and mesoscopic studies routinely show that such frictions disproportionately penalize motorists when the (5) window is tight [15], [16]. Consequently, the reported driving-mode Gini should be interpreted as a *lower bound* and overall reachability as optimistic, especially at 18–15 minutes, where queue growth is most explosive. By contrast, pedestrian flows are less (6) constrained by fixed intersection capacities and can spread across local streets and paths, so the free-flow assumption is less distortive for walking. These direction-of-bias statements frame the comparisons across modes and guide the reading of Δ-metrics for the Smile Hill alternative under compressed ETAs [36].

3. Results and Discussion

The inundation surface from the COMCOT scenario, thresholded at >0.30 m (robustness checked at >0.00 m), polygonizes into a small set of multipart features after dissolve, with clean topology once reprojected to EPSG:32748. Projected road-graph nodes that fall inside this extent constitute the at-risk set; counts of at-risk nodes by village match the global total, confirming consistent tagging and CRS harmonization (QC frames retained for the Supplement). This hazard overlay establishes the spatial domain for all subsequent accessibility and equity calculations.

Table 1 concentrates the headline indicators across ETA = 22, 18, 15 min and walking/driving. At 22 min, all at-risk origins reach a TEA in both modes (RR = 1.00) and inequality is minimal (Gini ≈ 0.008 (walk); ≈ 0.022 (drive)), with similarly low inequality Gini*. Tightening the window to 18 min reduces RR to ≈ 0.33 (walk) and ≈ 0.28 (drive) and elevates inequality (Gini ≈ 0.69–0.76), while Gini* rises further, indicating that shortfalls concentrate in more hazardous villages. Under 15 min**,** RR ≈ 0.04 in both modes with Gini ≈ 0.79 (and the highest Gini*)**.** The Smile Hill alternative produces no systemwide change at 18 or 15 min (ΔRR = ΔGini = ΔGini* = 0) and, because RR already saturates at 1.00 for 22 min, also leaves systemwide indicators unchanged at 22 min [36].

Table 1. Overall access and equity metrics

Mode	ETA (min)	RR_overall (Baseline)	Gini (Baseline)	Gini* (Baseline)	RR_overall (Smile Hill)	ΔRR	ΔGini	ΔGini*
Walk	22	1.00000	0.00834	-	-	-	-	-
Drive	22	1.00000	0.02210	-	-	-	-	-
Walk	18	0.32748	0.68830	0.35048	0.32748	0	0	0
Drive	18	0.28169	0.75747	0.43185	0.28169	0	0	0
Walk	15	0.04302	0.78639	0.55423	0.04302	0	0	0
Drive	15	0.04382	0.79491	0.53270	0.04382	0	0	0

Note: Because results assume **free-flow** (no link/intersection capacities, no queues), the reported driving-mode Gini values constitute a ***lower bound*** on real-world inequality; true inequality is likely higher and overall reachability lower under tight ETAs [7], [9], [10], [15], [16].

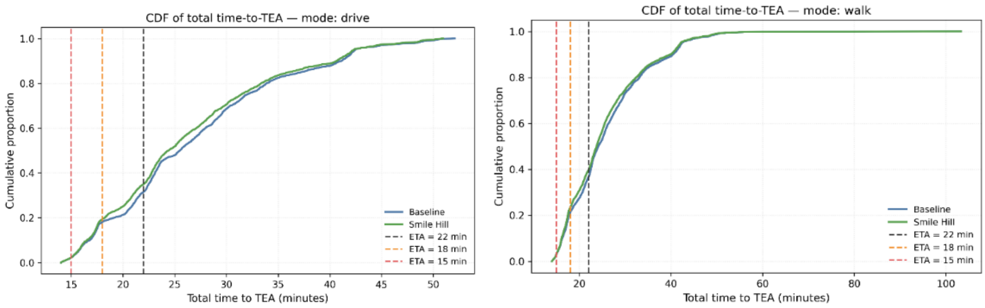

Figure 2. CDF of total time to TEA (a) drive mode and (b) walk mode ; ETA = 22/18/15 min.

Distributional evidence at ETA 22 corroborates these aggregates, and the multi-threshold view at ETA = 22/18/15 further clarifies the regime change. The cumulative distributions of total travel time ti for Smile Hill versus Baseline show a consistent leftward shift—shorter times for a subset of origins in both walking and driving while the dashed ETA lines (22/18/15) intersect progressively lower portions of the distributions—mid-mass at 22 min and lower-tail at 18/15 min; hence binary access remains unchanged at 22 min and system-level gains diminish as the budget tightens to 18/15 min (Figure 2A–B). This pattern—efficiency gains without a change in reachability—is characteristic of a plateau regime in near-field evacuation windows [7]–[9], [13], [14]. the 18/15-min behavior is consistent with a time-scarcity collapse [7]–[9], [13], [14]. The shift is more visible in walking than in driving, aligning with localized ΔRR for walking and near-zero ΔRR for driving; see the near-coastal constraint in the Hmax mask (Fig. 1) [36].

Cumulative distribution functions (CDFs) of total time to the nearest TEA for Baseline (blue) and Smile Hill (green). Vertical dashed lines indicate ETA = 22 (black), 18 (orange), and 15 (red) min (same color scheme as Fig. 2). Smile Hill shifts the distribution slightly left (lower times). Intersections with the three ETA lines imply limited change in binary access at 22 min and shrinking gains as the budget tightens to 18/15 min. Same setup as Fig. 2 for walking. The leftward shift relative to Baseline is more visible than in driving; however, at 22 min the threshold still intersects the mid-mass of the distribution (plateau-like binary access). At 18/15 min, curves converge, consistent with time-scarcity collapse and diminishing system-level gains

Isochrone catchments for driving under a 22-minute allowance. Baseline catchments (hatched teal) are overlaid with the Smile Hill alternative (solid blue), with existing TEAs shown as red stars and Smile Hill as a yellow star. The red coastal band indicates the Hmax mask (Fig. S1). Catchments largely cover the at-risk belt, with local expansions around Smile Hill along the west–central corridor—consistent with a plateau regime at 22 minutes.

Baseline catchments (hatched green) and the Smile Hill alternative (solid green) are shown; The Hmax coastal mask is shown in red. Walking coverage is broad and contiguous, with marginal local gains near Smile Hill, reinforcing that at 22 minutes the intervention redistributes effort rather than changing binary access

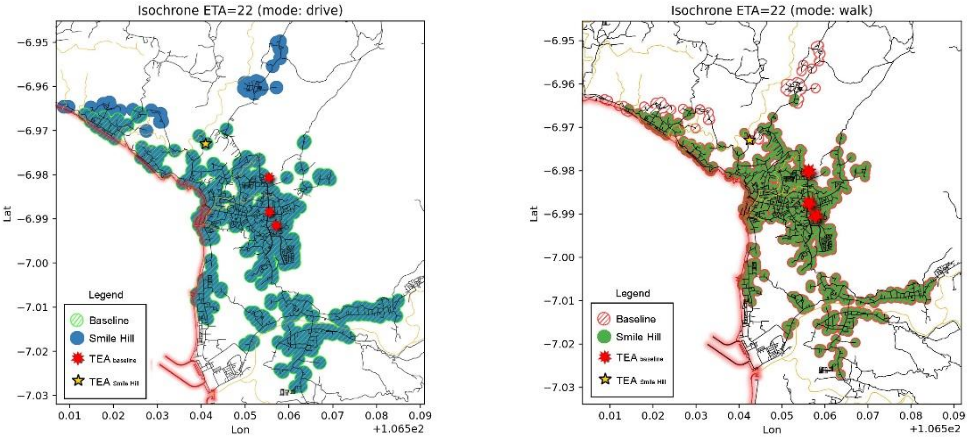

Figure 3. Isochrones, a): drive mode and b) walk mode ; ETA = 22 min.

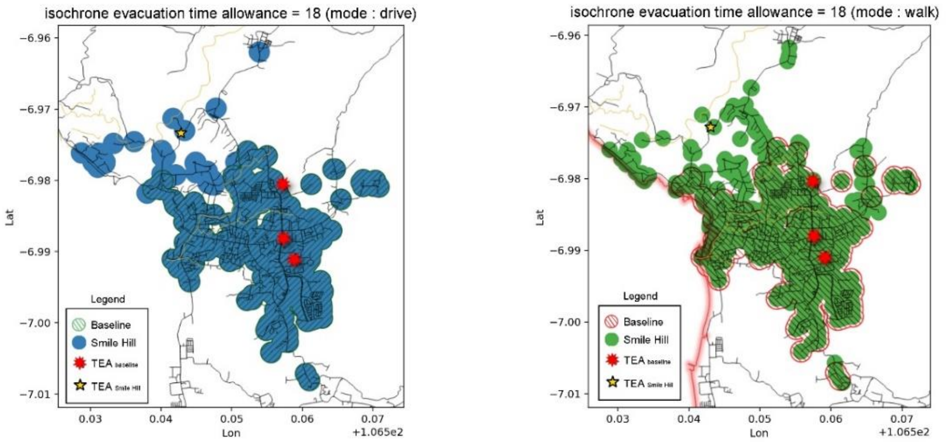

Figure 4. Isochrones, a) drive mode and b) walk mode ; ETA = 18 min.

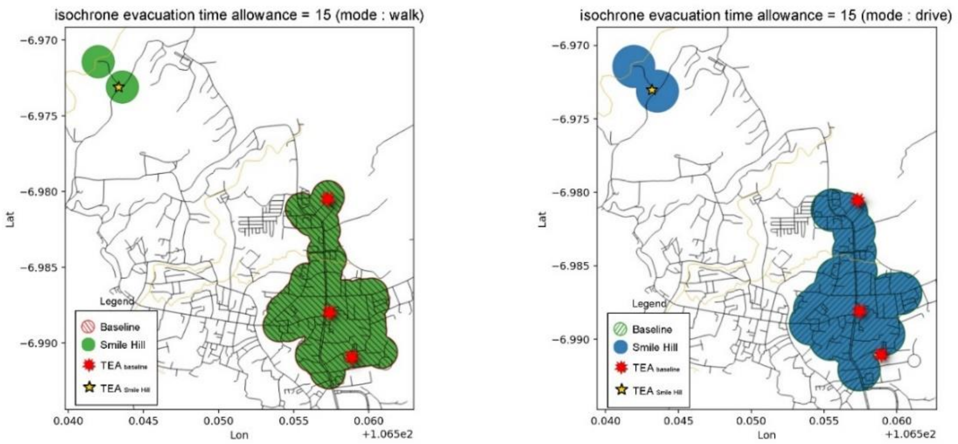

Figure 5. Isochrones, a) drive mode and b) walk mode ; ETA = 15 min.

As the time budget tightens to 18 minutes, drive catchments (blue) become highly fragmented and discontinuous. The Smile Hill TEA provides only a marginal expansion of local reach, while access from baseline TEAs becomes non-contiguous. This indicates time scarcity is beginning to dominate system-wide access

Figure 4. Isochrones, ETA = 18 min (mode: walk). Walking access (green) remains more contiguous than driving at 18 minutes, but catchments are visibly shrinking. The area around Smile Hill shows a tighter, more efficient local catchment (solid green), but the system is clearly bounded by the 18-minute budget, and gains do not propagate system-wide.

Figure 5. Isochrones, ETA = 15 min (mode: walk). The "collapse regime" is evident at 15 minutes. Walking catchments shrink to small, isolated pockets

around the baseline TEAs and the Smile Hill. Access is now purely local, confirming that a single-site addition has no systemic impact in such a highly constrained time window. Isochrones, ETA = 15 min (mode: drive). At 15 minutes, driving access is reduced to small, "islanded" polygons immediately surrounding the baseline TEAs and Smile Hill. System-wide access is effectively zero, illustrating a complete collapse dominated by extreme time scarcity.

Spatial isochrones (5-minute bands up to 22 min) clarify where those efficiency gains accrue. Envelopes for Smile Hill modestly expand or reshape relative to Baseline along corridors that connect directly to the additional TEA, whereas elsewhere the envelopes overlap closely, mirroring the CDF behavior Because all at-risk origins are already within the 22-minute budget, such expansions do not flip non-reachable origins into reachable ones, keeping RR at 1.00.

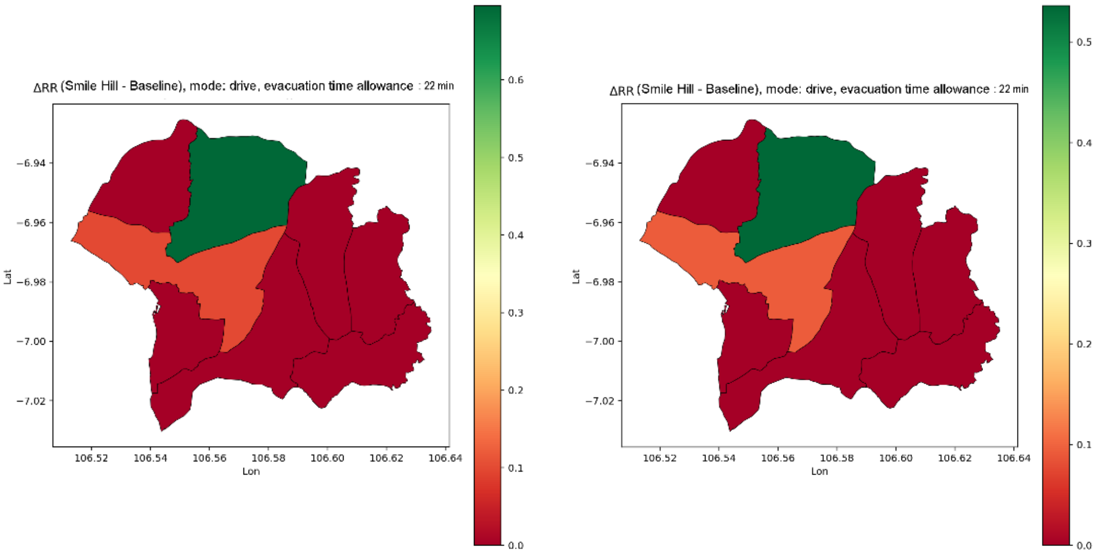

Figure 6. ΔRR (Smile Hill − Baseline), a): drive mode and b) walk mode ; ETA = 22 min.

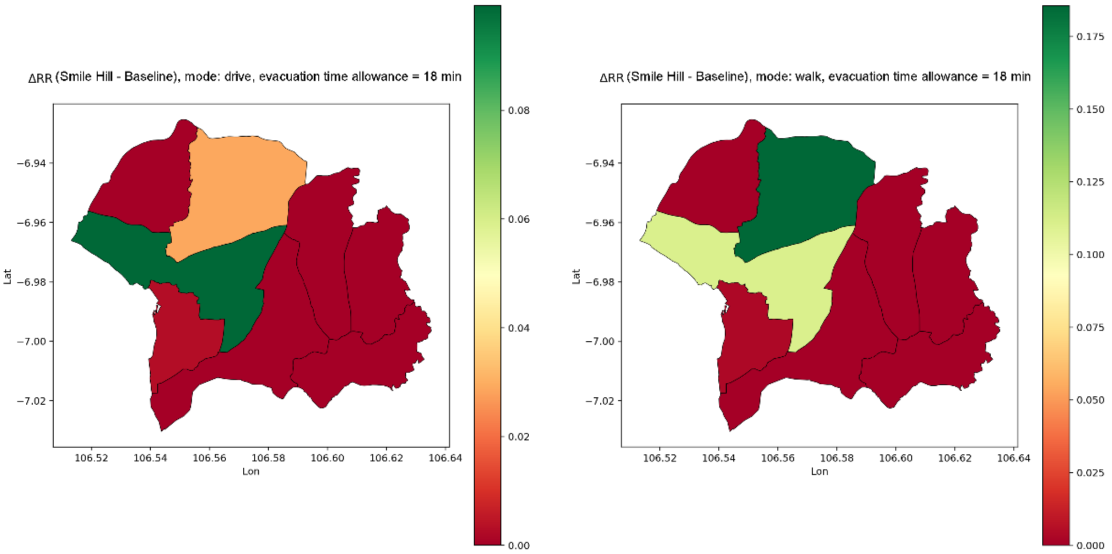

Figure 7. ΔRR (Smile Hill − Baseline), a): drive mode and b) walk mode ; ETA = 18 min.

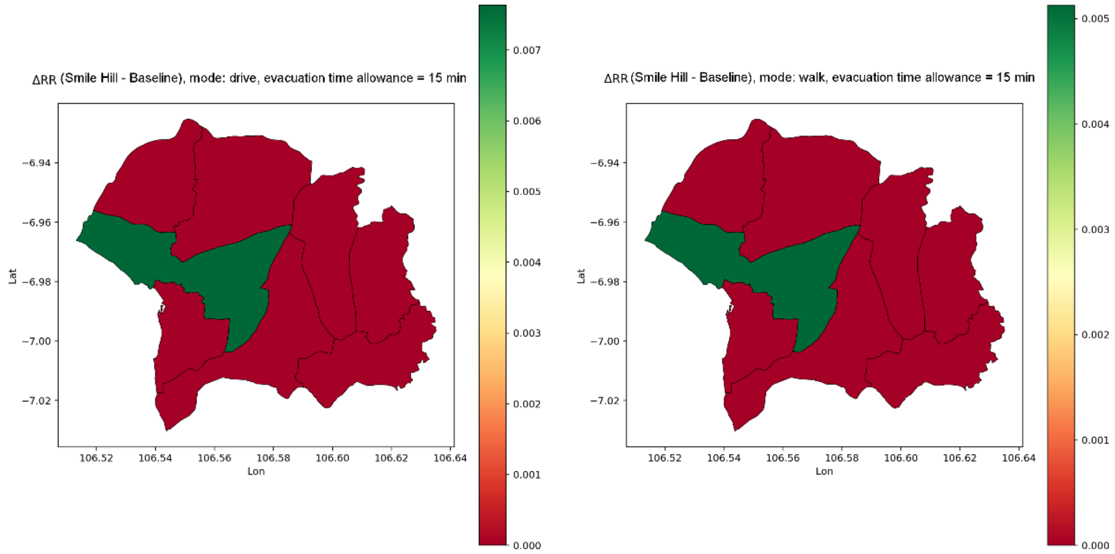

Figure 8. ΔRR (Smile Hill − Baseline), a): drive mode and b) walk mode ; ETA = 15 min.

Figure 6. ΔRR (Smile Hill − Baseline), mode: drive, ETA = 22 min. Village-level change in overall reachability (*ΔRR*) when the candidate *TEA* Smile Hill is added, driving mode, *ETA* = 22 min. Colors show gains: dark green ≈ large increases (≈0.30–0.60), orange ≈ modest increases (≈0.10–0.30), dark red ≈ negligible change (≈0). Improvements concentrate in the north–northwest and west-central belt, while most villages show near-zero change. Village-level ΔRR for the walking mode at ETA = 22 min. Gains are broader than in driving, with the west-central corridor and northern sector showing the strongest pockets (up to ≈0.50), whereas other areas remain near zero (dark red).

Figure 7. ΔRR (Smile Hill − Baseline), mode: drive ETA = 18 min.Village-level change in overall reachability (ΔRR) for driving at 18 min. Positive pockets appear along the west–central corridor and a moderate cluster in the north (up to ~0.08), while most polygons remain non-positive, indicating the network is time-limited at 18 min. For walking at 18 min, more extensive gains emerge, especially in the north and west–central belt, with ΔRR up to ~0.18; nevertheless, improvements remain localized and do not alter system-level access.

Figure 8. ΔRR (Smile Hill − Baseline), mode: drive, ETA = 15 min. Under the 15-min window, driving gains are sparse and confined to a narrow west–central corridor (ΔRR up to ~0.007); the collapse regime dominates, leaving most villages unchanged. For walking at 15 min, small positive pockets (up to ~0.005) are concentrated near the central corridor; elsewhere ΔRR is non-positive, confirming localized benefits only.

Village-level maps of ΔRRv at ETA 22 localize these benefits. A compact north-western cluster exhibits positive ΔRRv —villages proximate to corridors served more directly by Smile Hill—while most villages remain at Δ≈0 (Figure 4A–B). For 18 and 15 min, ΔRRv =0 everywhere, because time scarcity dominates: many origins exceed the budget regardless of one added TEA, so no village changes its binary status. A concise Top-N table of villages with the largest ΔRRv at 22 min can be placed in the Supplement (exported from the per-desa equity tables). To make these collapse dynamics explicit, we extend the visualization to ETA = 18 and 15 minutes for both modes (Figs. 3C–F) and summarize village-level ΔRR for those windows (Figs. 4C–F). Isochrones contract and fragment; ΔRR concentrates in small pockets, confirming a time-scarcity collapse and keeping siting effects local rather than systemic [36]

At ETA = 22 minutes, both modes achieve RR = 1.00, with a modestly higher inequality for driving (Gini ≈ 0.022) than walking (≈ 0.008). As the modeled allowance tightens to 18 and 15 minutes, the two modes exhibit similar reductions in RR under the free-flow abstraction. This similarity should not be read as evidence that the modes behave the same in practice. Walking feasibility is primarily constrained by distance and grade and can disperse over fine-grained local streets and paths, whereas motorized access is highly sensitive to intersection control, bridge bottlenecks, and queue formation. Because routing here assumes ideal, uncongested conditions, the reported driving-mode Gini must be interpreted as an idealized lower bound; with realistic capacity and queuing, inequality for driving would plausibly be higher and RR lower—especially under 18–15 minutes [7], [9], [10], [15], [16]. At 18 min, driving shows isolated positive pockets (ΔRR up to ~0.08), while walking exhibits broader yet localized gains (ΔRR up to ~0.18) along the west–central and northern belts. At 15 min, only small pockets persist—walk up to ~0.005, drive up to ~0.007—making the collapse regime explicit [36].

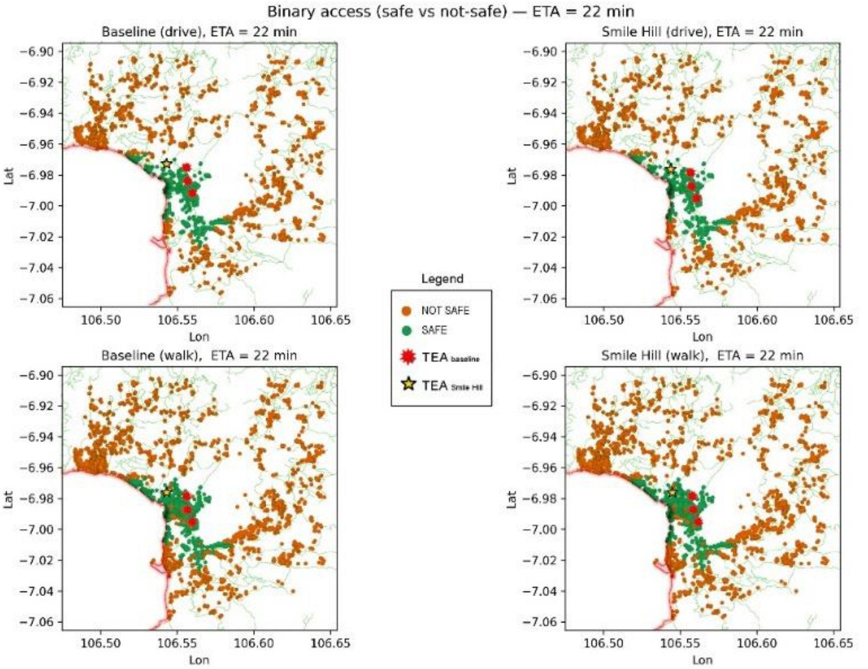

Figure 9. Binary access at ETA = 22 min

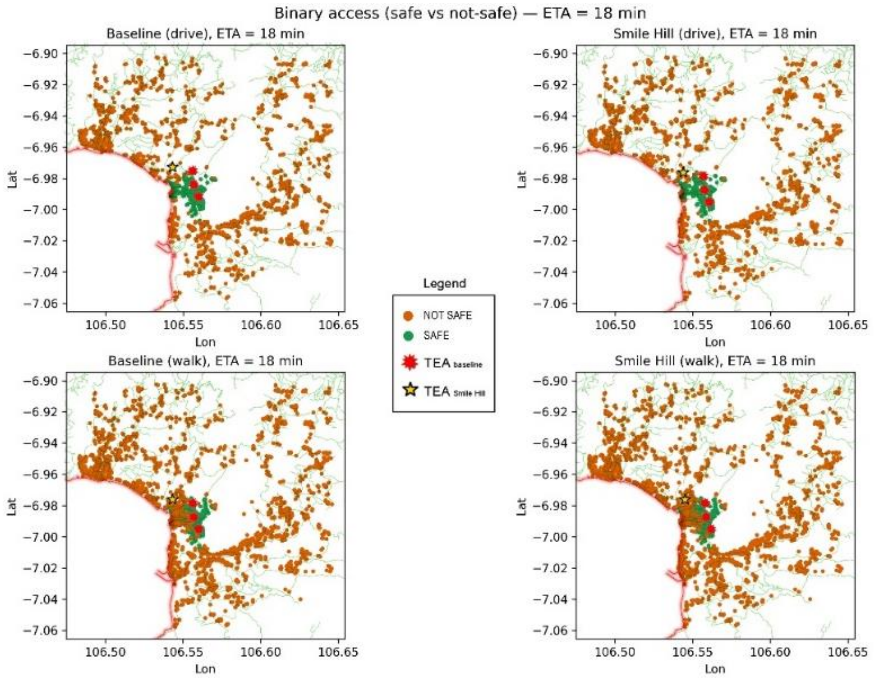

Figure 10. Binary access at ETA = 18 min

Four-panel comparison of binary access (safe vs not-safe) at ETA = 22 min. Top row: Baseline (drive) and Smile Hill (drive); bottom row: Baseline (walk) and Smile Hill (walk). Points are classified safe (green) if the least-time path to any TEA (plus notify/prepare buffers) ≤ ETA, and not-safe (orange) otherwise; roads are shown in light green and the red coastal swath is the Hmax mask (Fig. 9). The legend at the center summarizes symbolization, including baseline TEAs (red star) and the Smile Hill candidate (yellow star). Relative to the Baseline, Smile Hill yields localized conversions from orange to green near the west–central belt, more visible for walking than driving, but system-wide patterns remain broadly similar—consistent with small ΔRR (drive) and modest, localized ΔRR (walk) at 22 min [36].

Same layout as Fig. 9, Fig 10. for ETA = 18 min. Time scarcity emerges: only pockets near the central network show green, and the Smile Hill panels convert few additional origins, mainly within the near-coastal urban belt. Driving gains remain small; walking shows broader but still localized improvements. The scene aligns with the transition from plateau (22 min) toward collapse (≤18 min) described in the text [36].

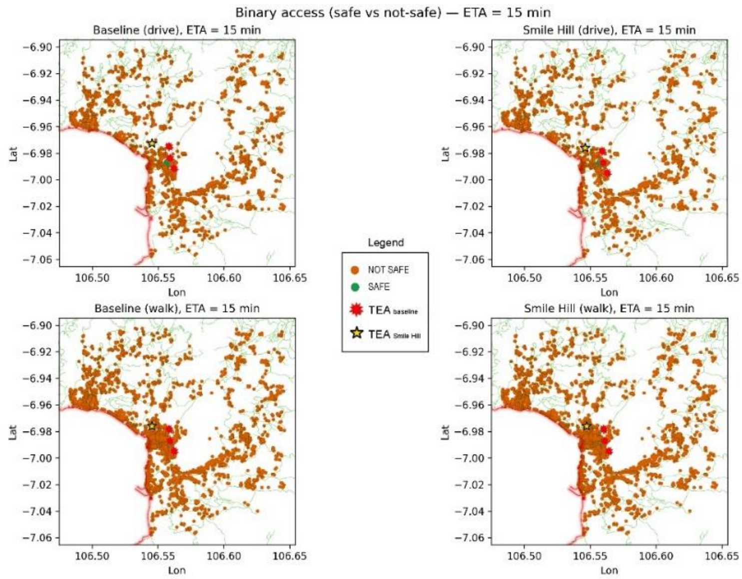

Figure 11. Binary access at ETA = 15 min

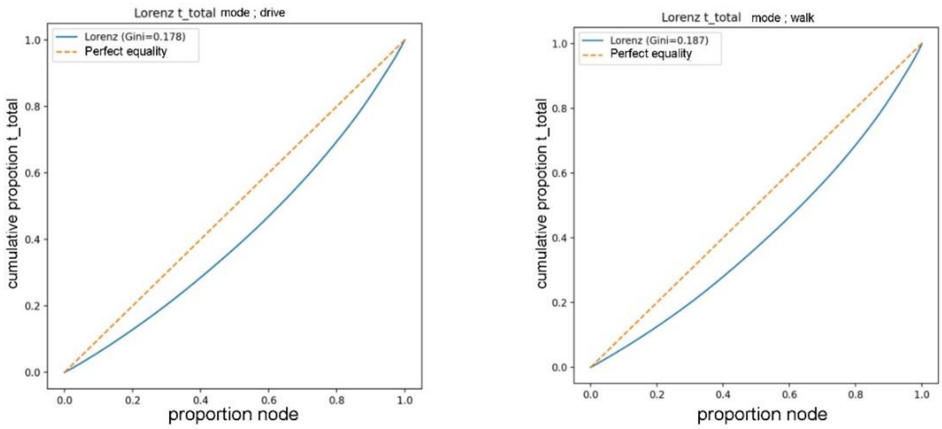

Figure 12. Lorenz curves of travel time (t_total) at ETA=22 min for (A) Driving and (B) Walking.

Figure 11. for ETA = 15 min, illustrating the collapse regime: most origins are not-safe for both modes; Smile Hill changes very few origins relative to Baseline. The composite emphasizes that under tight time budgets the network is capacity/time-limited, and design changes at a single TEA produce minimal system-level shifts, consistent with vanishing ΔRR and unchanged Gini/Gini* at 15 min

Figure 12. visualizes the inequality of effort (travel time) required to reach safety, even when overall reachability is perfect (RR=1.00). The x-axis represents the cumulative proportion of at-risk nodes, and the y-axis shows the cumulative proportion of the total travel time required for all nodes to evacuate. The dashed orange line represents a scenario of perfect equality, where all nodes have the identical travel time. Where RR = 1.00, inequality of effort can still be non-negligible. Lorenz curves of t_i at 22 indicate that the distribution of travel times remains left-concentrated yet unequal—slightly more so in driving—consistent with flow-path modelling in the evacuation literature [8], [9]. Sensitivity checks confirm that the inundation cutoff (0.00 vs. 0.30 m) does not alter outcomes at 18/15 min, and that the walking-speed sweep (2.0–3.5 km h^{-1}) leaves ΔRR effectively flat at 22 min (uniform heatmap, omitted from the body to avoid redundancy).

Taken together, the results form a coherent sequence: the COMCOT-based hazard overlay defines a compact at-risk domain; Table 1 shows plateau at 22 min and collapse at 18–15 min; Figure 2 (CDFs) andFigure 3 -5 (isochrones) explain why Smile Hill yields time savings but no system wide access change at 22 min; and pinpoints where small village-level gains occur. The evidence to ETA = 18/15 min, clarifying that gains remain local and largely vanish at 15 min; importantly, these additions do not alter the equity conclusions (RR, Gini, Gini*), but make the plateau→collapse transition explicit. All findings align with the empirically observed and nationally modelled sensitivity to lead-time compression in near-field settings [7]–[10], [13], [14], [21], [5] while keeping the interpretation of mechanisms for the dedicated Discussion that follows.

The results indicate a temporal tipping typical of near-field evacuation. With a generous allowance (ETA = 22 min), the system reaches an access plateau: every at-risk origin attains a TEA (RR = 1.00) and inequality is minimal. Tightening the allowance to 18 and 15 min pushes many origin–destination pairs beyond feasible limits, producing pronounced reductions in RR and a marked rise in distributional inequality. Viewed through the reachability function $R(T) = \frac{|\{i \in A : t_i \leq T\}|}{|A|}$,the response is sigmoid-like, with large marginal gains ∂R/∂T in the 18–22 min band and near-zero gains once the plateau is entered. This pattern is consistent with beat-the-wave logic and recent path-distance/ETE evidence showing that small lead-time reductions can flip large populations from reachable to non-reachable status [7]–[10], [13], [14]. The added panels at ETA = 18/15 (Figs. 3C–F and 4C–F) make this collapse regime explicit: isochrones contract and fragment and village-level ΔRR concentrates in small pockets, confirming that impacts are local rather than systemic under tight windows.

The juxtaposition of Table 1 with Figures 2–5 clarifies the mechanics of the plateau. At 22 min, adding the Smile Hill TEA shifts the travel-time CDF to the left and locally expands isochrones along corridors that connect efficiently to the new site; yet binary access is unchanged because the 22-minute threshold still lies to the right of the support of ti. In effect, the intervention reduces effort (minutes to safety) but not status (reachable vs. not)—a classic case of diminishing returns when the time budget already satisfies BTW requirements [8], [9], [13]. The spatial imprint of these efficiency gains is highly localized: a compact north-western cluster shows positive ΔRRv reinforcing that single-site additions mostly re-route flows within an existing envelope rather than expanding that envelope system-wide under generous ETAs. This reading aligns with the reproducible screening rubric used in the study (outside the Fig. S1 Hmax mask; connected to existing roads; near baseline deficit clusters) and with the equity constraints reported in the results—system-level RR/Gini/Gini* remain unchanged in substance, while local pockets reflect feasible but non-systemic improvements at 22 min [36].

The equity perspective adds a second dimension. Village-weighted Gini rises sharply as the allowance tightens, indicating that access losses are unevenly distributed. The Gini* increases faster still, showing that shortfalls concentrate where exposure (mean h_{max}) is higher. This pairing—coverage (RR) with a distributional metric (Gini) and, where relevant, exposure re-weighting—follows recent recommendations in transportation-equity and emergency-access scholarship and keeps vulnerable places visible in aggregated indicators [10]–[13]. Under 15–18 min, the joint movement of RR downward and Gini* upward signals a regime change from broadly shared access to selective access that favors better-connected or less-exposed villages.

Two robustness checks guide interpretation. First, results are insensitive to small inundation-extent choices (0.00 vs 0.30 m) at 18 and 15 min: performance is governed by time-to-safety, not modest planform differences. Second, the walking-speed sweep leaves *ΔRR* effectively flat at 22 min, consistent with the plateau reading. Both observations accord with national path-distance analyses that emphasize the primacy of lead time and departure delay; real-event evidence from the 2024 Noto Peninsula tsunami—departures within ~2–6-minutes [3] from large-scale smartphone geolocation—underscores how quickly pre-movement erodes the effective travel budget in near-field settings [7], [9], [10], [14], [36].

Mode comparisons corroborate these mechanisms but should be interpreted with care. At 22 min, walking and driving both achieve RR = 1.00, with driving showing slightly higher Gini**,** plausibly reflecting more heterogeneous impedance from one-way restrictions, bridge approaches, and circuitous arterials. As the allowance tightens to 18–15 min**,** the two modes exhibit similar reductions in RR under the free-flow abstraction**;** however, the real-world mechanisms differ**:** pedestrians can diffuse over fine-grained street fabrics and informal paths, whereas motorists concentrate on limited arterials and bridges where queues and spillback develop. Because routing here assumes ideal, uncongested conditions, the reported driving-mode Gini is an idealized *lower bound* on inequality, and driving-mode RR is likely optimistic—particularly at 18–15 min**,** where capacity and queuing would penalize motorists more strongly [7], [9], [10], [15], [16], [36].

Heterogeneity in on-foot evacuation further nuances these findings. Real outcomes depend on who evacuates and where they must climb: cohorts with larger shares of older adults or persons with disabilities move more slowly and with higher variance; group walking and child accompaniment introduce coordination delays absent in a constantspeed abstraction [4], [7], [18]. Where slopes steepen near TEAs, effective walking speed diminishes and path choices concentrate, shrinking the reachable set and amplifying between-village differences tied to terrain [5]. Thus, even though free-flow assumptions are less distortive for walking than for driving, the reported walking Gini is also conservative with respect to demographic and topographic variability; explicit modeling of $v_{walk}(x)$ would plausibly increase inequality through mechanisms distinct from capacity-driven penalties.

Crucially, the 18–22-minute range identified here is a case-specific tipping window shaped by Palabuhanratu's arrival timing, network geometry and grade, TEA layout, and the screening model's free-flow abstraction. In other settings, R(T) may shift left or right with earlier/later arrivals, denser or more circuitous street fabrics, alternative siting (including vertical evacuation), demographic speed distributions, and jurisdictional warning/pre-movement delays; capacity and queuing would further reshape outcomes under tight windows [7]–[10], [13], [14], [15], [16]. Hence the form of the curve and the equity patterns likely generalize, but the numeric thresholds demarcating plateau versus steep decline are not universal and require site-specific calibration. Policy implications & next steps. In the same RR–Gini–Gini* frame we outline: (i) replacing a single allowance with a spatial lead-time field ETA (x,y); (ii) targeted congestion/capacity penalties at critical bridges/intersections; (iii) uncertainty bands for RR, Gini, Gini* from a compact hazard ensemble; and (iv) lightweight validation/transfer checks (e.g., drill notes or anonymized traces; one additional town) — all modular and reproducible. [7]–[10], [13], [14]. Our added 18/15-min panels operationalize this guidance: they show how tightening windows drives a time-scarcity collapse (fragmented isochrones; near-zero ΔRR) while leaving the triad's system-level conclusions intact. This clarifies when local siting adjustments redistribute effort at 22 min versus when tighter budgets require different levers (e.g., portfolio/vertical options or lead-time gains) [36].

These strands offer an organizing picture for design questions (kept here at the research level). When the system resides on the plateau **(**22 min**),** local siting adjustments can lower travel times and redistribute effort without altering who reaches safety; portfolio questions (e.g., multiple TEAs, vertical options) become more pertinent if the goal is to change binary access**.** When the allowance enters a tight-window regime (**≤** 18 min), time scarcity dominates: ΔRR_v vanishes across the map and inequality rises fastest where exposure is greatest. In such settings, the RR–Gini–Gini***** triad remains useful because it compactly couples how many**,** how fairly, and where hazard is highest**,** enabling reproducible comparisons across ETA**,** mode**,** and configuration [7]–[10], [13]–[16], [36].

4. Conclusion

A network-based equity evaluation for Palabuhanratu shows a clear temporal structure to tsunami evacuation performance. With a 22-minute budget, the system resides on an access plateau: all at-risk origins reach a TEA and distributional inequality is low. Compressing the allowance to 18 and 15 minutes induces a collapse regime in which reachability falls sharply and inequality—especially its hazard-weighted form—rises fastest in the most exposed villages. These signatures are consistent with *beat-the-wave* logic and contemporary path-distance/ETE evidence on the primacy of lead time and departure delay in near-field settings [7]–[10], [13], [14], [36].

Within this temporal framing, the alternative site (Smile Hill) delivers localized time savings and small positive changes in village-level reachability at 22 minutes but no systemwide change at 18 or 15 minutes. Under generous budgets, siting tweaks redistribute effort (minutes) rather than status (reachable vs. not); under tight budgets, time scarcity overwhelms local improvements, making ΔRR_v vanish across the map. Mode comparisons corroborate the mechanism: walking and driving both plateau at 22 minutes and both collapse as the window tightens; the slightly higher inequality in the driving mode underlines the role of circuitous arterial geometry, a gap that real-world congestion and blockages would likely amplify [15], [16], [36].

Methodologically, the paper contributes a compact, reproducible screening triad**—**RR**,** Gini, and Gini*— that joins *how many*, *how fairly*, and *where hazard is highest* into a single comparative frame across ETA**,** mode**,** and TEA configuration**.** Built on a physics-based inundation field and open road graphs, the pipeline is transparent and transferable, allowing other coastal districts to benchmark their own TEA options with the same indicators [1], [2], [5], [6].

Three implications follow. First, when planning assumptions or local arrival times support a 22-minute envelope, portfolio questions (multiple TEAs, including vertical evacuation) are more relevant than single-site tweaks if the goal is to change binary access rather than merely shorten routes. Second, where communities routinely face 18–15 minute constraints, interventions that expand lead time (warning issuance, pre-movement reduction, drills) may dominate spatial siting effects—a conclusion aligned with national-scale modelling and recent event evidence [7]–[10], [13], [14]. Third, reporting hazard-weighted inequality alongside coverage should become standard practice so that access shortfalls in higher-exposure places remain visible in headline indicators.

The analysis is deliberately a deterministic screening**.** Future extensions should incorporate multi-scenario hazard ensembles**,** heterogeneous ETA fields (arrival-time surfaces), and capacity/congestion/obstruction dynamics to convert technical travel time into operational estimates. Even so, within its scope the study isolates the governing control—time-to-safety—and provides a replicable equity lens for rapid TEA appraisal in near-field tsunami settings [7]–[10], [13]–[16]. Under these free-flow assumptions, the driving-mode inequality we report should be treated as a *lower bound*; with realistic capacity and congestion dynamics**,** inequality would be higher and reachability lower—especially at 18–

15 minutes—which would further reinforce the temporal-tipping narrative [7], [9], [10], [15], [16]. In closing, the study answers the original question by showing that Palabuhanratu's evacuation performance hinges on a temporal regime: a 22-min plateau where siting redistributes effort locally without status change, and a 18/15-min collapse where time scarcity dominates. Policy-wise, TEA placement should therefore be screened not only for spatial coverage but for time consistency with expected arrivals. Within the same reproducible pipeline, promising next steps include evaluating vertical or portfolio TEAs, multimodal access plans, and pre-movement reduction, while continuing to report the RR–Gini–Gini* triad to keep equity visible.

Suggestion

The detailed policy options and parameter extensions have been consolidated in Discussion — Policy implications & next steps ETA (x,y); targeted capacity/queue terms; uncertainty bands; lightweight validation/transfer) and are evaluated within the same reproducible, equity-centric RR–Gini-Gini* frame.

Acknowledgement

We gratefully acknowledge the OpenStreetMap contributors (© OpenStreetMap, ODbL 1.0) for road-network data and GADM (v4.1) for administrative boundaries. We thank the developers and maintainers of the open-source tools that enabled this work—OSMnx and NetworkX for network construction and routing; GeoPandas**,** Shapely, PyOgrio/Fiona**,** Rasterio**,** and PROJ/pyproj for geospatial processing; and NumPy**,** Pandas, and Matplotlib for analysis and visualization. We also acknowledge the COMCOT tsunami modelling community for documentation and guidance that informed the inundation layer used here. The authors appreciate the constructive input from local stakeholders in Palabuhanratu who shared contextual knowledge and TEA information. Any remaining errors are the authors' responsibility.

References

[1] X. Wang, *Comprehensive Modelling of Coastal Tsunamis (COMCOT) – User's Guide and Model Physics*, 2009. (software manual)

[2] X. Wang and W. Power, "COMCOT model and its applications," *GNS Science Report*, 2011. (tech. report)

[3] F. Makinoshima, S. Yotsui, S. Sato, and F. Imamura, "Massive geolocation data reveal evacuation behaviour during the 2024 Noto Peninsula earthquake and tsunami,", 2024, doi:10.48550/arXiv.2412.05795

[4] H. Kim, S. Park, S. Hamdar, and P. R. Stopher, "An agent-based simulation for tsunami evacuation: Waikīkī, Hawaiʻi," *Transportation Research Part D*, vol. 110, 103239, 2022, doi:10.1016/j.trd.2022.103239.

[5] N. Wood, C. Jones, and M. Schmidtlein, "Pedestrian flow-path modeling to support tsunami evacuation and disaster relief planning in the U.S. Pacific Northwest," *International Journal of Disaster Risk Reduction* Volume 18, September 2016, 41–55, 2016, doi.org/10.1016/j.ijdrr.2016.05.010.

[6] Wood, N.J., Peters, J., Sheehan, A.F., Bausch, D., 2025. "National population exposure and evacuation potential in the United States to earthquake-generated tsunami threats". *International Journal of Disaster Risk Reduction* 123, 105511. https://doi.org/10.1016/j.ijdrr.2025.105511

[7] F. Makinoshima and F. Imamura, "Milling and evacuation departure time distributions in the 2011 Tohoku tsunami," *International Journal of Disaster Risk Reduction*, vol. 111, 104673, 2024, doi:10.1016/j.ijdrr.2024.104673.

[8] J. León, A. Ogueda, L. Hurtado, A. Gubler, and N. Zamora, "An integrated framework for analysing horizontal and vertical tsunami evacuation: Iquique, Chile," *International Journal of Disaster Risk Reduction*, vol. 116, 105140, 2024. doi.org/10.1016/j.ijdrr.2024.105137

[9] E. Mas, L. Moya, E. Gonzales, and S. Koshimura, "Reinforcement learning-based tsunami evacuation guidance system," *International Journal of Disaster Risk Reduction*, vol. 115, p. 105023, Dec. 2024. doi.org/10.1016/j.ijdrr.2024.105023

[10] T. Takabatake, K. Asai, H. Kakuta, and N. Hasegawa, "Optimizing evacuation paths using agent-based evacuation simulations and reinforcement learning," *International Journal of Disaster Risk Reduction*, vol. 117, p. 105173, Feb. 2025.doi.org/10.1016/j.ijdrr.2024.105173

[11] N. Ahmed, J. Jui, D. Liu, K. Kim, J. Kim, and J. Lee, "Understanding inequalities in geographic accessibility to emergency cyclone shelters in Bangladesh under climate change," Journal of Transport Geography, vol. 123, p. 104134, Feb. 2025. doi.org/10.1016/j.jtrangeo.2025.104134

[12] A. Karner, R. H. M. Pereira, and S. Farber, "Advances and pitfalls in measuring transportation equity," *Transportation*, vol. 52, pp. 1399–1427, 2025, doi:10.1007/s11116-023-10460-7.

[13] B. van Wee and T. de Jong, "Differences in levels of accessibility: The importance of spatial scale when measuring distributions of the accessibility of health and emergency services," *Journal of Transport Geography*, vol. 106, p. 103511, Jan. 2023. doi.org/10.1016/j.jtrangeo.2022.103511

[14] K. Martens, "Equity considerations in transport planning," in *International Encyclopedia of Transportation, R. Vickerman, Ed. Amsterdam,*

Netherlands: Elsevier, 2021. doi.org/10.1016/B978-0-08-102671-7.10634-7
[15] M. A. Giannotti, J. Barros, D. B. Tomasiello, D. Smith, B. Pizzol, C. Zhong, B. M. Santos, Y. Shen, E. C. L. Marques, and M. Batty, "Inequalities in transit accessibility: Contributions from a comparative study between Global South and North metropolitan regions," *Cities*, vol. 109, p. 103016, 2021. doi.org/10.1016/j.cities.2020.103016
[16] A. Berke, W. Truitt, and K. Larson, "Is access to public bike-share networks equitable? A multiyear spatial analysis across 5 U.S. Cities," *Journal of Transport Geography*, vol. 108, p. 103579, Mar. 2023. doi.org/10.1016/j.jtrangeo.2023.103759
[17] J. León, A. Gubler, P. Catalán, M. Correa, J. Castañeda, G. Beninati, and A. Ogueda, "Assessing potential tsunami vertical-evacuation practices: A study of four cases in Chile using virtual reality and GIS," *International Journal of Disaster Risk Reduction*, vol. 108, p. 104098, Mar. 2024. doi.org/10.1016/j.ijdrr.2023.104098
[18] A. Muhammad, R. De Risi, F. De Luca, W. Kongko, N. Mori, T. Yasuda, dan K. Goda, "Integrated tsunami risk framework considering agent-based evacuation modelling: The case of Saga, Kochi Prefecture, Japan," *International Journal of Disaster Risk Reduction*, Art. no. 104193, Des. 2023. doi.org/10.1016/j.ijdrr.2023.104193
[19] Liu, C., Lindell, M.K., Wang, H., 2025. "'Households' expected and actual preparation times in tsunami evacuation drills International" *Journal of Disaster Risk Reduction* 129, 105767. doi.org/10.1016/j.ijdrr.2025.105767
[20] Y. Yang, J. Yin, W. Feng, L. E. Yang, dan J. Wang, "Dynamic flood evacuation modelling for coastal cities: A case study of Shanghai," *International Journal of Disaster Risk Reduction*, Art. no. 105591, Jul. 2025. https://doi.org/10.1016/j.ijdrr.2025.105591
[21] Wood, N. J., Jones, J. L., Peters, J., & Richards, K., 2018. Pedestrian-evacuation modeling to reduce vehicle use for distant tsunami evacuations in Hawaiʻi. *International Journal of Disaster Risk Reduction*, 28, 271–283. doi.org/10.1016/j.ijdrr.2018.03.009
[22] National Tsunami Hazard Mitigation Program, 2023. United States National Tsunami Hazard Mitigation Program Strategic Plan for 2024–2029. National Oceanic and Atmospheric Administration, National Weather Service, 31 pp + supplements.
[23] International Code Council, *2024 International Building Code—Appendix M: Tsunami-Generated Flood Hazards*, 2024. (code)
[24] A. Abraham, Y. Zhang, and S. Prasad, "Evacuation Management Framework towards Smart City-wide Intelligent Emergency Interactive Response System," arXiv preprint arXiv:2403.07003 [cs.AI], 2024, doi.org/10.48550/arXiv.2403.07003
[25] F. Marinelli, A. Pizzuti, G. Romano, G. Bernardini, and E. Quagliarini, "An ILP formulation to optimize flood evacuation paths by minimizing pedestrian speed, length and effort," arXiv preprint arXiv:2504.12958 [physics.soc-ph], 2025. doi.org/10.48550/arXiv.2504.12958
[26] Data layers: Global Administrative Areas (GADM) v4.1, 2024–2025. Available: https://gadm.org (accessed 2025).
[27] Street network: OpenStreetMap Contributors, 2025. Available: https://www.openstreetmap.org (accessed 2025).
[28] G. Boeing, "OSMnx: New methods for acquiring, constructing, analyzing, and visualizing complex street networks," *Computers, Environment and Urban Systems*, vol. 65, pp. 126–139, 2017, doi:10.1016/j.compenvurbsys.2017.05.004.
[29] A. A. Hagberg, D. A. Schult, and P. J. Swart, "Exploring network structure, dynamics, and function using NetworkX," in *Proc. 7th Python in Science Conf. (SciPy 2008)*, pp. 11–15, 2008, doi:10.25080/TCWV9851.
[30] C. R. Harris, K. J. Millman, S. J. van der Walt, et al., "Array programming with NumPy," *Nature*, vol. 585, pp. 357–362, 2020, doi:10.1038/s41586-020-2649-2.
[31] The pandas development team, *pandas (v1.x) [Software]*, Zenodo, 2020, doi:10.5281/zenodo.3509134.
[32] J. D. Hunter, "Matplotlib: A 2D graphics environment," *Computing in Science & Engineering*, vol. 9, no. 3, pp. 90–95, 2007, doi:10.1109/MCSE.2007.55.
[33] The GeoPandas contributors, *GeoPandas v0.10.1 [Software]*, Zenodo, 2021, doi:10.5281/zenodo.5555834.
[34] S. Gillies et al., *Rasterio: Geospatial raster I/O for Python programmers* (software), 2013–, GitHub project page (accessed 2025).
[35] Snow A. D., Whitaker J., et al., 2010–2025. pyproj/PROJ – cartographic projections and coordinate transformations library for Python, version 3.x, available at: https://pyproj4.github.io/pyproj
[36] Indira, I., & Manessa, M. D. M. (2023). "Generating Evacuation Route for Tsunami Evacuation Based on Megathrust Scenario Hazard Model in Palabuhanratu Village, Sukabumi, West Java". *International Journal of Disaster Management*, 6(1), 35-48 doi.org/10.24815/ijdm.v6i1.31148